

# Longitudinal Analysis of Human Pancreatic Adenocarcinoma Development Reveals Transient Gene Expression Signatures



Jungsun Kim<sup>1,2,3</sup>, Taelor Ekstrom<sup>2</sup>, Wenli Yang<sup>4</sup>, Greg Donahue<sup>5</sup>, Dmytro Grygoryev<sup>2</sup>, Thuy T.M. Ngo<sup>1,2,6</sup>, John L. Muschler<sup>3,6</sup>, Terry Morgan<sup>2,7</sup>, and Kenneth S. Zaret<sup>5</sup>

## ABSTRACT

Previous transcriptome studies of human pancreatic ductal adenocarcinoma (PDAC) compare non-cancerous pancreatic intraepithelial neoplasias (PanIN) with late-stage PDAC obtained from different patients, thus have limited ability to discern network dynamics that contribute to the disease progression. We demonstrated previously that the 10-22 cell line, an induced pluripotent stem cell–like line reprogrammed from late-stage human PDAC cells, recapitulated the progression from PanINs to PDAC upon transplantation into NOD/LtSz-scid/IL2R-gamma<sup>null</sup> mice. Herein, we investigated the transition from precursor to PDAC using the isogenic model. We analyzed transcriptomes of genetically tagged 10-22 cells progressing from PanINs to PDAC in mice and validated the results using The Cancer Genome Atlas PDAC dataset, human clinical PanIN and PDAC tissues, and a well-established murine PDAC model. We functionally studied candidate proteins using human normal (H6C7) and cancerous (Miapaca2, Aspc1) pancreatic ductal epithelial cell lines. 10-22 cell–derived PDAC displayed

the molecular signature of clinical human PDAC. Expression changes of many genes were transient during PDAC progression. Pathways for extracellular vesicle transport and neuronal cell differentiation were derepressed in the progression of PanINs to PDAC. HMG-box transcription factor 1 (HBP1) and BTB domain and CNC homolog 1 (BACH1) were implicated in regulating dynamically expressed genes during PDAC progression, and their expressions inversely correlated with PDAC patients' prognosis. Ectopic expression of HBP1 increased proliferation and migration of normal and cancerous pancreatic cells, indicating that HBP1 may confer the cell dissemination capacity in early PDAC progression. This unique longitudinal analysis provides insights into networks underlying human PDAC progression and pathogenesis.

**Implications:** Manipulation of HBP1, BACH1, and RUN3 networks during PDAC progression can be harnessed to develop new targets for treating PDAC.

## Introduction

A better understanding of the development and progression of pancreatic ductal adenocarcinoma (PDAC) will inform better diagnoses and therapies (1). Pancreatic intraepithelial neoplasias (PanIN) are major PDAC precursors (2) and are classified as low grade (PanIN1

and 2) and high grade (PanIN3) based on cytologic atypia severity. Low-grade PanINs are considered clinically benign, whereas high-grade PanINs, usually found in pancreata with PDAC, are regarded as carcinoma *in situ* (2). PanIN2 is the earliest lesions that harbor genetic alterations in *KRAS*, *CDKN2A*, and *TP53* typically seen in PDAC (3, 4). PanIN3 and PDAC share common mutations, whereas PDAC-specific mutations other than those in *SMAD4* appear to be passengers (5, 6).

Gene expression in human PanINs (7–9), PDAC (10–19), and PDAC cell lines (20) has been investigated. The transcriptome studies revealed two major PDAC subtypes, a basal (or squamous) subtype with a worse prognosis and a classical subtype with a better prognosis (12–15). Different cell populations in PDAC have been characterized using an intraductal transplantation model (21). However, most works with human samples did not longitudinally compare gene expression in individual isogenic series. Although genetic mutational profiling can reveal cancer evolution (5, 19, 22, 23) and the pseudotemporal ordering of single cells can suggest lineages (24), the pseudotemporal order of cancer cells can be confounded by undocumented genetic changes. Thus, an analysis of transitions from human PanINs to their corresponding PDAC is currently lacking. Genetically engineered mouse models (25) have provided the basis for studying the phenotypic manifestation of defined genetic mutations. However, most transcriptome studies of these models compare normal with cancer (26) or acinar to ductal conversion (27–29), thus not revealing the dynamic process.

We previously created an induced pluripotent stem cell (iPS)-like cell line (designated 10-22) from a recurrent advanced stage of PDAC. Despite having mutations, including an activating *KRAS* mutation, heterozygous deletion of *CDKN2A*, and decreased *PTEN* and *DPC4* copy number as well as 20 of the 23 chromosomal rearrangements

<sup>1</sup>Department of Molecular and Medical Genetics, Oregon Health & Science University School of Medicine, Portland, Oregon. <sup>2</sup>Cancer Early Detection Advanced Research Center, Knight Cancer Institute, Oregon Health & Science University School of Medicine, Portland, Oregon. <sup>3</sup>Knight Cancer Institute (Cancer Biology Research Program), Oregon Health & Science University School of Medicine, Portland, Oregon. <sup>4</sup>Department of Medicine, Institute for Regenerative Medicine, University of Pennsylvania Perelman School of Medicine, Philadelphia, Pennsylvania. <sup>5</sup>Institute for Regenerative Medicine, Department of Cell and Developmental Biology, Abramson Cancer Center (Tumor Biology Program), University of Pennsylvania Perelman School of Medicine, Philadelphia, Pennsylvania. <sup>6</sup>Department of Biomedical Engineering, Oregon Health & Science University, Portland, Oregon. <sup>7</sup>Department of Pathology, Oregon Health & Science University, Portland, Oregon.

**Note:** Supplementary data for this article are available at Molecular Cancer Research Online (<http://mcr.aacrjournals.org/>).

**Corresponding Author:** Jungsun Kim, Department of Molecular & Medical Genetics, Cancer Early Detection Advanced Research Center, Knight Cancer Institute, Oregon Health & Science University, Portland, OR 97239. Phone: 503-346-1967; E-mail: kimjungsu@ohsu.edu

Mol Cancer Res 2021;19:1854–67

doi: 10.1158/1541-7786.MCR-21-0483

This open access article is distributed under Creative Commons Attribution-NonCommercial-NoDerivatives License 4.0 International (CC BY-NC-ND).

©2021 The Authors; Published by the American Association for Cancer Research

presented in the original tumor (30), 10-22 cells develop into PanIN2/3 by 3 months and then into PDAC by 9 months when injected into NOD/LtSz-scid IL2R-gamma<sup>null</sup> (NSG) mice (30). Furthermore, ductal lesions are surrounded by human stromal cells that are also differentiated from 10-22 cells. The system revealed an HNF4a-driven network specific to the early to intermediate stages of PDAC (30) and a biomarker, THBS2, that can discriminate patients with resectable or advanced stages of PDAC from healthy controls (31).

In this study, we sought to gain insights into gene networks during the progression of human PanINs to PDAC. We tagged 10-22 cells with the KiR-EG reporter vector that expresses GFP from a ubiquitous promoter and a near-infrared fluorescent protein (iRFP; ref. 32) from a duct-selective K19 promoter (33) then injected tagged cells into NSG mice. We monitored lesions *in vivo* over time by iRFP fluorescence and used GFP<sup>+</sup>iRFP<sup>+</sup> cells of the pancreatic ductal epithelial lineage isolated at different timepoints for RNA sequencing (RNA-seq) analysis. Our unique ability to capture events in isogenic, longitudinal tumor development allowed us to identify effectors and networks associated with the progression of early PanINs to PDAC.

## Materials and Methods

### PanIN and PDAC mouse model

All animal works were performed with the Institutional Animal Use and Care Committee (IACUC) approval of the Oregon Health & Science University School of Medicine (OHSU). Ages 2–2.5 and 4–6 months old PDAC mice (*p48-Cre; LSL-KrasG12D/+; Trp53R172H*; ref. 25) were analyzed for *HBPI* expression at the PanINs and tumor stages, respectively. All transgenic lines used were backcrossed at least five generations onto the C57Bl/6J background, and female and male mice are used.

### Culturing 10-22 cells, generation of KiR-EG vector, labeling 10-22 cells, and gating strategy

The KiR-EG lentiviral vector was constructed to express iRFP (32) driven by the keratin 19 (K19) gene promoter (33) in the backbone of GFP driven by a ubiquitous EF1a promoter to produce a lentivirus from 293T cells (30). The 10-22 cells were cultured as described previously (30). Comparative genomic hybridization, karyotyping, and exome sequencing were performed to authenticate 10-22 cells. 10-22 cells were transduced with KiR-EG lentivirus, various subclones were isolated, and their expressions of GFP and iRFP were validated by FACS. Each 10-22 cell tagged with KiR-EG was subcutaneously transplanted into 4–6 weeks old female NSG mice as described previously (30) with UPenn IACUC approval. The tumor growth was measured for up to 9 to 10 months by iRFP using Xenogen IVIS Spectrum in Penn Small Animal Imaging Facility. *Mycoplasma* test was routinely performed every 3 months in each cell line and lower passages (15–25) of 10-22 KiR-EG cells were used.

For RNA-seq, lesions were resected under a fluorescence dissecting microscope at 1 week, 2 weeks, 3 months, 6 months, and 9 months after injection. FACS sorted GFP-positive (GFP<sup>+</sup> and GFP<sup>+</sup>iRFP<sup>+</sup>) cells. A small portion of tissues was fixed in 4% paraformaldehyde for histology evaluation and the rest was dissociated as single cells (30). As a negative control for FACS, contralateral control (CLC) tissue of the same mice was used. As CLC did not show significant background signals in either GFP or GFP/iRFP compared with mouse embryonic fibroblasts (MEF), we isolated GFP, GFP/iRFP, and double-negative (mouse host) cells with consistent gate parameters across all lesions and clones.

### RNA-seq and data processing

Pooled cDNA libraries, generated from total RNA, were sequenced using NextSeq500 sequencer and the trimmed reads were aligned to the hg 19 genomes using STAR (34). HTSeq count was used to quantify tags over genes (Supplementary Table S2), then normalized and called differentially expressed (DE) genes (*FDR Benjamini-Hochberg adjusted  $q < 0.05$* ) between two pairwise samples by Wald test or among all the samples across each time-point by likelihood-ratio test (LRT) using DESeq2 package (35). Homer motif analysis (36) identified *de novo* Transcription factor (TFs) bind to promoters (1,000 bp upstream of transcription start site) of genes within selected Ward cluster groups. RNA-seq data are available on NCBI GSE173286 and GSE173489. RNA-seq and data processing codes are available on Code Ocean (Capsule #6902043) and Github ([https://github.com/gdonahue/Kim\\_MCR\\_2021](https://github.com/gdonahue/Kim_MCR_2021)). Detailed analysis is available in the Supplementary Data. Additional results are available in supplementary figures and tables as resource datasets.

### Comparison of 10-22 cells gene expression datasets to other datasets

The Cancer Genome Atlas (TCGA) PDAC RNA-seq dataset ( $n = 150$ ; ref. 37), which ranked genes based upon RSEM values from 0% to 100% (“IlluminaHiSeq percentile” dataset), was downloaded (38). Nonlinear dimensionality reduction method, multidimensional scaling (MDS) was performed with cmdscale in R package. To compare with human pluripotent embryonic stem cells (ESC), rank-ordered FQ values of human ESC (39), the third quartile SAGE tags of human ESCs tags (40), and Progenitor Cell Biology Consortium (PCBC) RNA-seq dataset, which contains gene expression data from 48 pluripotent stem cells (7 ESC lines, 41 iPSC lines) and their differentiated cell populations (41), were used. The PCBC data code is publicly available on GitHub.

### Kaplan-Meier survival analysis of TCGA PDAC dataset

The cutoff for *HBPI* expression was determined by equally segregating TCGA PDAC cohorts (37) into two groups at 10.57 (log<sub>2</sub> transformed normalized RSEM) because the range of *HBPI* expression level was evenly spread across the PDAC cases. To determine the cutoff for *BACH1* expression, we examined the risk table with three different *BACH1* log<sub>2</sub>-transformed normalized RSEM levels (from the first quartile to the third quartile) because *BACH1* is expressed abundantly in many PDAC cases and then stratified the survival curve with 10.27, the value in the 75th percentile.

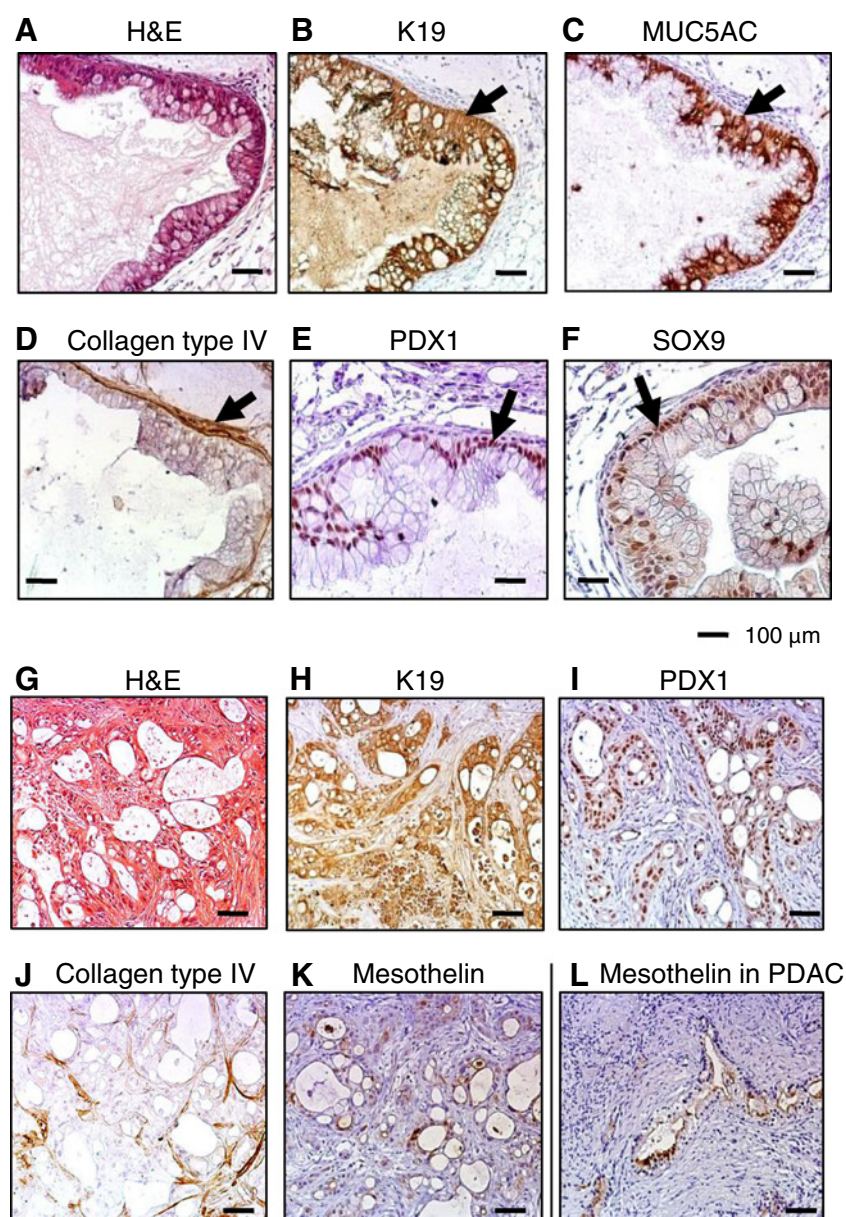
### HBPI CRISPR-cas9 targeting

AsPC-1 cells were transfected with two CRISPR-Cas9 vectors targeting the RB-binding domain of *HBPI* exon 2 (gRNA#1, gRNA#2). Transfected cells were selected using 5 µg/mL puromycin for 48 hours, cultured for 2 more weeks without puromycin, then examined for the deletion of *HBPI* using Sanger sequencing.

## Results

### PanINs derived from 10-22 cells resemble human disease

We confirmed the stepwise PDAC progression of 10-22 cells after transplantation into NSG mice. Six of the 7 NSG mice injected with 10-22 cells developed PanINs that express K19, MUC5AC, PDX1, and SOX9 by 1.5 to 3 months (Supplementary Table S1A; Fig. 1A–F). PanINs possessed an intact collagen IV+ basement membrane (Fig. 1D; ref. 42). Tumors grown *in vivo* for 13 months showed highly

**Figure 1.**

Pancreatic lesions developed in NSG mice transplanted with 10-22 cells. **A-F**, hematoxylin and eosin (H&E) staining (**A**) and IHC for human-specific K19 (**B**), MUC5AC (**C**), collagen IV (**D**), PDX1 (**E**), and SOX9 (**F**) of PanINs developed in NSG mice 3 months after transplanted with 10-22 cells. **G-L**, H&E staining (note: H&E staining was pinker than normal H&E as the tumors secreted high abundant collagen that eosin preferentially binds; **G**), IHC for human-specific K19 (**H**), PDX1 (**I**), collagen IV (**J**), and mesothelin (**K**) of PDACs developed in NSG mice 13 months after 10-22 cell transplantation, and IHC for mesothelin in a human PDAC serving as a positive control (**L**). Arrows in **B-F** indicate positive staining of markers. Scale bars indicate 100  $\mu$ m.

dysmorphic (**Fig. 1G**) K19<sup>+</sup>, PDX1<sup>+</sup>, and mesothelin<sup>+</sup> structures with collagen IV<sup>+</sup> basement membrane breakdown ( $n = 3/4$ ; **Fig. 1H-K**). Mesothelin is a marker for advanced PDAC (**Fig. 1L**; ref. 43). After 13 months, 3 of 4 mice exhibited additional tumors that migrated beyond the injection sites (Supplementary Table S1B). These findings demonstrate that 10-22 cells can recapitulate PanINs, invasive, and migratory phenotypes with features common to those documented for clinical human PDAC.

#### PDACs derived from 10-22 reporter subclones are histologically heterogeneous

PanINs and PDAC express K19, 10-22 cells express K19 upon ductal differentiation but they also differentiate into other lineages (30). To isolate ductal and non-ductal 10-22 cells from mouse cells, we developed the lentivirus KiR-EG vector that expresses iRFP driven by a K19 promoter (33) and GFP driven by an EF1a promoter (**Fig. 2A**;

Supplementary Fig. S1A). We labeled 10-22 cells with KiR-EG lentivirus and isolated clones that gave rise to iRFP and GFP double-positive cells during *in vitro* differentiation (Supplementary Fig. S1B). Four stable KiR-EG clones were injected into NSG mice individually and their growth was followed for 9 months. Clones #6 and #9 generated PanINs followed by PDAC like the parental 10-22 cells, and thus they were chosen for detailed analysis (**Fig. 2B-D**; Supplementary S1C-S1E, S2, and S3A). While various cell types were seen in lesions at 1 week after injection, PanIN-like ductal epithelial structures were enriched by 1 to 3 months after injection and became increasingly heterogeneous over time (Supplementary Fig. S2 and S3A). For example, after 6 months, mouse 8560 RT had a well-differentiated tumor with a relatively intact basement membrane, whereas mouse 5074T had a poorly differentiated tumor (Supplementary Fig. S2). Tumors greater than 4 mm in diameter *in vivo* are detectable by their iRFP signal (**Fig. 2F**; Supplementary Fig. S3B). In sum, we validated

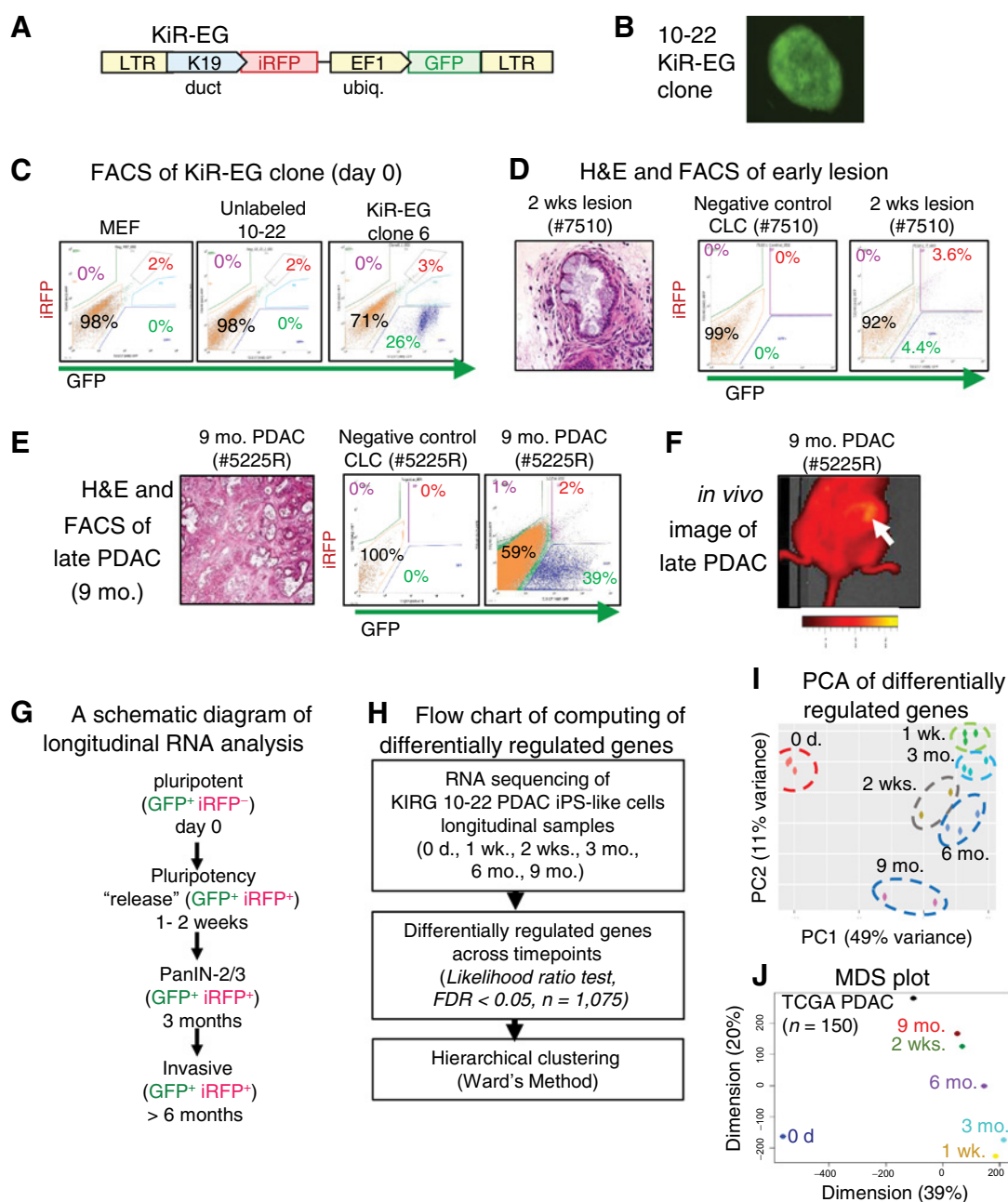


**Figure 2.** Longitudinal transcriptome analysis of 10-22 cells *in vivo*. **A**, Schema of the KiR-EG lentiviral vector. **B**, A representative image of 10-22 cells tagged with KiR-EG-expressing GFP in the pluripotent culture condition (day 0). **C**, A FACS plot for GFP and iRFP expression of KiR-EG clone 6 (day 0). MEF and unlabeled 10-22 cells are negative controls. **D**, H&E staining image and FACS plot of the early lesion (#7510) occurring 2 weeks after injecting KiR-EG clone 6. CLC from the same mouse was used as a negative control. **E**, H&E image and FACS plot of late PDAC (#5225) arose by nine months after injecting the KiR-EG clone. **F**, Optical imaging for the iRFP signal of a 9-month tumor (#5225). Bar indicates radiant efficiency and color scale from 2.32e6 to 3.44e7. Arrow indicates the iRFP tumor. **G**, A schematic diagram of a longitudinal RNA analysis. **H**, Flow chart for computing DE genes. **I**, PCA of DE genes. **J**, MDS plots of *in vivo* lesions derived from 10-22 KiR-EG cells and 150 TCGA PDAC.

that 10-22 KiR-EG clones recapitulate the PDAC progression of their parental 10-22 cells.

**Identify PDAC progression-associated gene signatures**

To characterize the global gene expression during the transition from iPS-like cells to PanINs and PDAC, we performed RNA-seq on

iRFP<sup>+</sup>/GFP<sup>+</sup> cells, representing the ductal lineage, from 10-22 KiR-EG clone 6 at 1 week, 2 weeks, 3 months, 6 months, and clones 6, 9, and 10 at 9 months after transplantation into NSG mice (Fig. 2G). GFP<sup>+</sup> cells at day 0 were used as controls.

On the basis of histology of the lesions (Supplementary Fig. S2), we defined each stage with RNA-seq replicates as follows; undifferentiated

iPS stage (day 0, triplicates), released from near-pluripotency (1 week after transplantation, triplicates; and 2 weeks after transplantation, duplicates), PanINs (3 months after transplantation, triplicates), early invasive PDAC (6 months after transplantation, triplicates), and PDAC (9 months after transplantation, duplicates). Spearman rank correlation coefficient with log-transformed normalized DESeq2 counts indicated a strong correlation between biological replicates in each timepoint, including across different clones at the 9-month timepoint (Supplementary Fig. S3C).

To identify stage-specific gene signatures in the 10-22 PDAC progression model, we discovered 1,075 DE genes across all the timepoints using the LRT ( $FDR < 0.05$ ; Fig. 2H; Supplementary Table S2). PCA and Euclidian clustering showed that the earliest differentiated population (1 week) was located the farthest from day 0, indicating rapid differentiation of 10-22 cells after transplantation (Fig. 2I; Supplementary Fig. S3D). Moreover, undifferentiated 10-22 cells were located most closely to late-stage tumors (9 months), consistent with reported similarities between pluripotent and cancer cells (Fig. 2I; Supplementary Fig. S3D; ref. 44). Similar results were observed when we percentile ranked the gene expression values of 10-22 KiR-EG clone 6 and its differentiated counterparts and compared them with the percentile ranked-ordered gene expression values of 150 TCGA PDAC RNA-seq datasets (37) by MDS ( $n = 150$ ; Fig. 2J). To avoid ubiquitously expressed genes and focus on pathologically relevant genes, we studied genes enriched between the 75th and 92nd percentile of expression (38), which varied the most highly across samples. PDAC can be classified into classical and basal subtypes based on gene expression (12–15). Clustering normalized counts with the PDAC-subtype gene signatures (15) showed that 10-22 cell-derived PDAC at 9 months had a classical and basal hybrid subtype (Supplementary Fig. S4A and S4B). Altogether, we validated that the 10-22 PDAC progression model reflected the heterogeneity observed in natural PDAC (14, 45).

We then assessed the expression of genes associated with pluripotency, endoderm, oncogenesis, and tumor suppression. The majority of Muller pluripotent genes (44) were expressed in the starting 10-22 cells and downregulated by 1 week after transplantation, as expected (Supplementary Fig. S4C). Endodermal genes such as *KRT19*, *SOX9*, *HNF1B*, and *FOXA3* were upregulated by 2 weeks of transplantation (Supplementary Fig. S4D). While *KRAS* was consistently expressed across timepoints, with transient downregulation 3 months after transplantation, *CDKN2A*, *TP53*, and *BRCA1/2*, known to contribute to PDAC development (3, 4), variously expressed during PDAC development (Supplementary Fig. S4E).

### 10-22 cells retain the memory of the pancreatic epithelial lineage

We rank-ordered transcripts by their expression levels in undifferentiated 10-22 KiR-EG clone 6 and compared them with the ranked-ordered transcripts of human ESCs (39). The Spearman rank-order correlation coefficient (0.60) and the coefficients of linear regression (0.79; Supplementary Fig. S4F) were consistent with our original observation that 10-22 cells were different from ESCs (30). Unexpectedly, early endodermal genes *FOXA1*, *GATA4*, and *GATA6* were clearly expressed in undifferentiated 10-22 cells (Supplementary Fig. S4D), indicating that 10-22 cells retain endodermal gene signatures in the iPS-like stage (30). To further investigate genes aberrantly upregulated in 10-22 cells compared with normal ESCs, we compared the top 20% of rank-ordered genes in 10-22 cells with the bottom 20% rank-ordered genes in human ESCs. These 129 genes aberrantly expressed in undifferentiated 10-22 cells were enriched with the Gene

Ontology (GO) associated with epithelium development, regulation of microvillus organization, endodermal origin small airway epithelium, and PDGF pathway (Supplementary Table S3C). The signature was enriched for malignant neoplasia, including pancreatic cancer (ref. 46;  $q < 0.05$ ; Supplementary Table S3C), indicating the memory of the pancreatic cancer epithelial state in 10-22 cells. In summary, 10-22 cells express both pluripotency networks and polarized endodermal epithelial cell networks, suggesting how they tend to develop into the pancreatic epithelial lineage (30).

### Genes dynamically expressed in the 10-22 PDAC progression model show distinct gene signatures at different stages

We clustered DE genes from 10-22 derivatives into five stage-specific signatures based on the expression pattern across timepoints using Ward method (Fig. 3A; ref. 47). It showed a gene signature specific to the 10-22 KiR-EG clone 6 cultured in pluripotent conditions (group 1; Fig. 3A). While most group 1 genes (Supplementary Fig. S5A and S5B) expressed higher in pluripotent ESCs and iPSCs, some ( $n = 51$ ) expressed less in pluripotent ESCs compared with their differentiated counterparts (Supplementary Fig. S5B and S5C). Comparing group 1 genes with the published RNA-seq (39) and third quartile-SAGE tags (40) from human ESC confirmed that group 1 genes significantly overlap with genes explicitly expressed in pluripotent ESCs (Supplementary Fig. S6). The expressed genes in group 1 were enriched with GO terms associated with cell-cycle regulation ( $q < 8E-21$ ; Supplementary Fig. S5C; Supplementary Table S3A). The deletion of these genes generally causes early embryonic lethality (ref. 48;  $q < 2.89E-03$ , top 10 phenotypes; Supplementary Fig. S5C; Supplementary Table S3B). The group 2 genes, whose expression oscillated over time (Fig. 3A;  $n = 213$ ), were involved in epigenetic regulation ( $q < 0.05$ ; Supplementary Table S3D).

The expression of group 3 genes gradually increased over time and stayed up at 9 months (Fig. 3A), reflecting the late PDAC stages. GO terms showed that group 3 genes are enriched to cell adhesion ( $n = 13/44$ ,  $q < 0.05$ ; Fig. 3B) including extracellular matrix (ECM) features ( $q = 1.69E-04$ ), consistent with ECM remodeling in later stages of PDAC progression (Supplementary Table S3E). Validating this finding, 30 of 44 group 3 genes that are highly expressed in TCGA PDAC are enriched in malignant neoplasms ( $q < 0.05$ ; Fig. 3C; ref. 46). Thus, we confirm that 10-22-derived tumors display adenocarcinoma gene signatures by 9 months, particularly with ECM remodelers. These findings agree with the breakdown in collagen IV basement membrane structures in late-stage 10-22 tissue (compare Fig. 1D and J) and further validate the model system.

### The KRAS pathway and extracellular vesicle transports are reactivated early in the 10-22 PDAC progression model

Upon differentiation, 10-22 cells upregulated a small portion of basal subtype signature (Supplementary Fig. S4B), which correlates with the amplification of *KRAS*-mutant alleles (15). Nevertheless, upon differentiation, 10-22 cells developed PanIN-like lesions that undergo PDAC progression and profoundly increase their classical subtype signatures in 9-month samples (Supplementary Fig. S4A). We thus asked how the classical subtype gene program can override the default basal cell fate.

We examined groups 4 and 5 genes that covered PanINs and early invasive stages during 10-22 PDAC progression. Group 4 genes include genes increased at the earliest differentiation upon 10-22 cells being released from pluripotency (1 week) and remained until early invasive stages (6 months; Fig. 3A). As expected, GO terms of group 4 genes enriched signal pathways activated in response to external cues

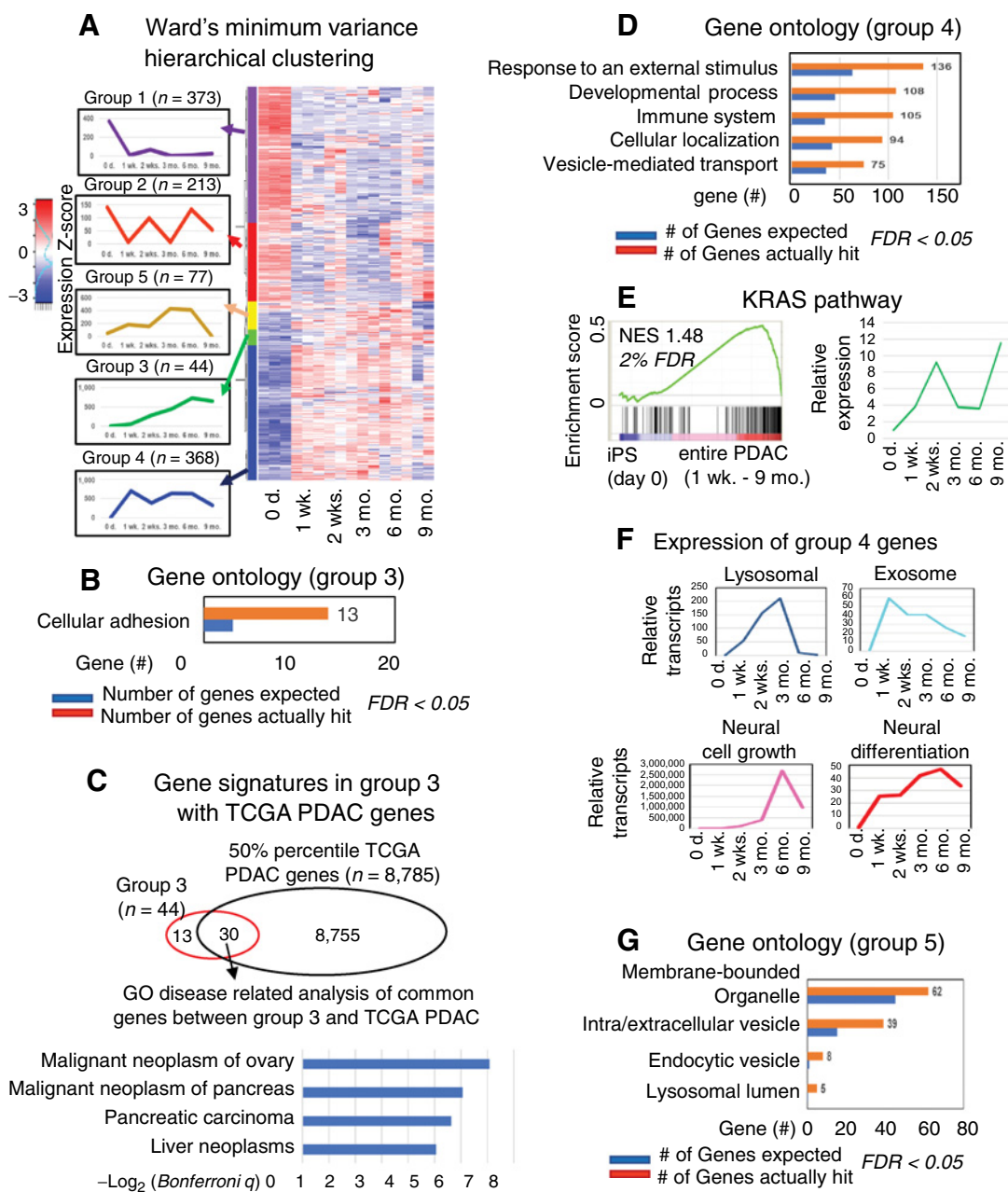


**Figure 3.**

Gene signatures associated with the early lesions to invasive stages. **A**, Ward minimum variance hierarchical clustering of DE genes across timepoints computed by LRT ( $FDR < 0.05$ ). The heatmap indicates Z-score expression. **B**, Representative GO categories of genes in group 3 ( $n = 44$ ). **C**, Comparison of genes in group 3 with those in TCGA PDAC. **D**, Representative GO categories of genes in group 4 ( $n = 368$ ). **E**, GSEA of KRAS pathway in the entire PDAC programmed cells (1 week–9 months) after 10-22 KiR-EG cells were transplanted into NSG mice (left) and relative median expression level of genes in the KRAS pathway over day 0 (right). **F**, Expression of group 4 genes involved in lysosomal, exosome, and neural development. Y-axis shows the relative median expression level over day 0. **G**, Representative GO categories for group 5 genes ( $n = 77$ ).

upon differentiation and developmental processes ( $n = 368$ ; **Fig. 3D**; Supplementary Table S3F). Consistently, gene set enrichment analysis (GSEA) showed activation of KRAS pathways as early as 1 week (Supplementary Table S5A) and throughout the entire PDAC progression after transplantation, compared with day 0 (**Fig. 3E**; Supplementary Table S5B). This agrees with the well-established role of mutant KRAS, such as the G12D mutation in 10-22 cells, as an early

driver of PDAC progression (30). Genes involved in lysosomal membrane protein and exosomes were rapidly upregulated upon differentiation (**Fig. 3F**). Although lysosomal activity (49–51) and exosome pathways (52) play key roles in human PDAC, it was unclear whether they occur early in the disease, that is, higher in PanINs than in PDAC. Our data suggest that such cell-intrinsic networks can establish a microenvironment that is favorable to cancer progression early. On the

other hand, we found that genes in neural stem cell proliferation, neuronal differentiation, and neural invasion-driving chemokines (53, 54) were expressed the highest in early invasion stages (6 months) during PDAC progression of 10-22 cells (Fig. 3F).

The extracellular vesicle pathway was also enriched in group 5 genes, which arise slower than group 4 genes during the 10-22 PDAC progression (Fig. 3A-G). Products of most group 5 genes were associated with membrane-bound organelles (80%,  $n = 62$ ), and half of them (39 of 77 genes) are related to vesicle transport ( $q = 3.60E-06$ , fold enrichment 2.51; Fig. 3G; Supplementary Table S3G), including extracellular vesicles ( $n = 30$ ,  $q = 4.36E-02$ ).

Altogether, neuronal development, lysosomal membrane, and exosome gene programs were derepressed during the transition from precursor to invasive PDAC in the 10-22 cell model.

**HBPI is involved in cell migration pathways, and high HBPI mRNA level in PDAC is associated with poor prognosis of patients**

To identify transcriptional regulators associated with the progression of PanIN to early PDAC, we performed motif analysis of the promoters of groups 4 and 5 genes. The HBPI (55) motif ranked the highest among the group 4 genes ( $P = 1e-91$ ; Fig. 4A and B;

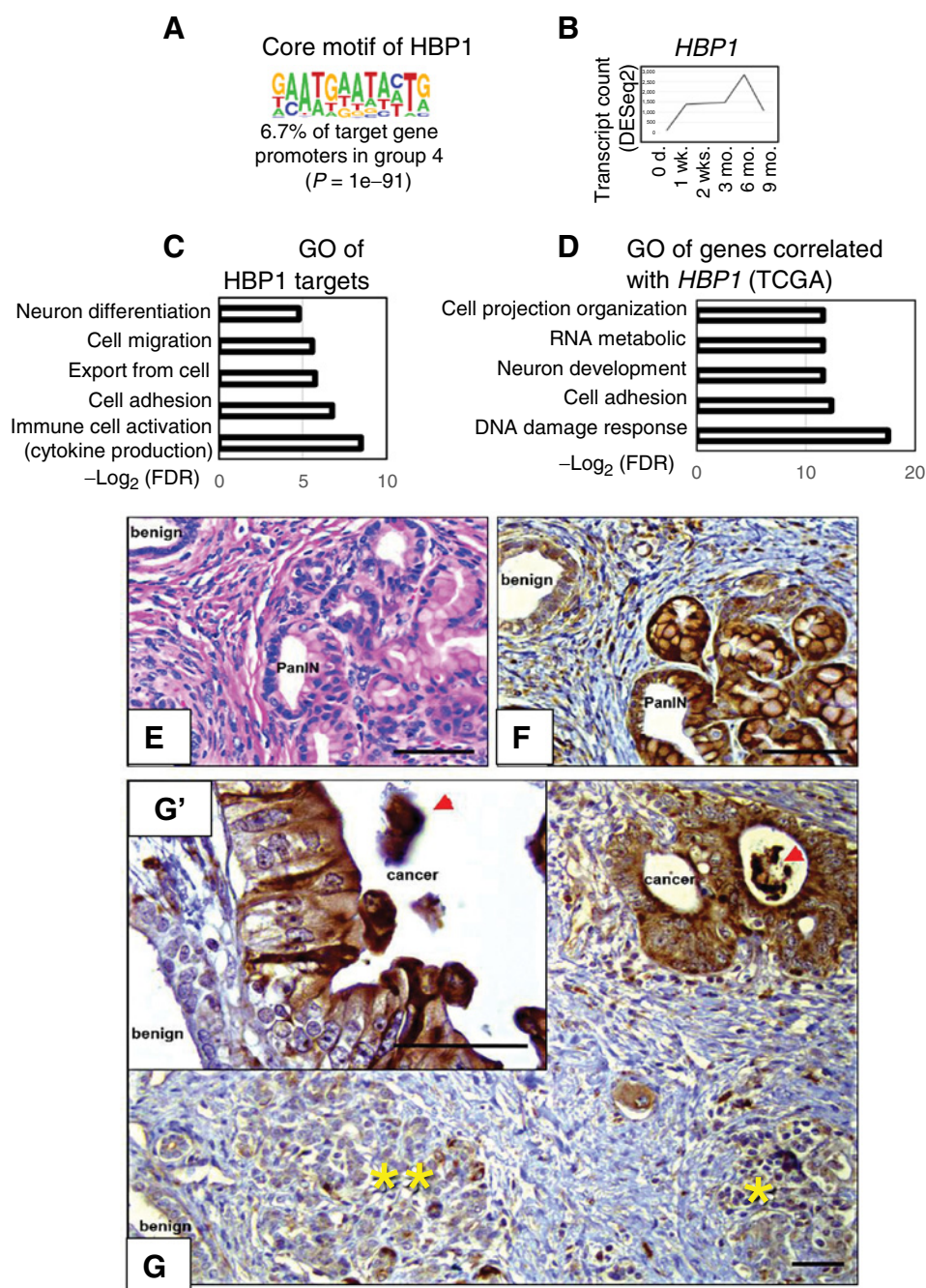


**Figure 4.** Enrichment of HBPI early in PDAC progression. **A**, HBPI motif. **B**, HBPI mRNA expression during PDAC progression of 10-22 cells. Representative GO categories for HBPI target genes (**C**) and genes correlated with HBPI in TCGA PDAC (**D**). H&E staining of PanINs and benign ductal mucosa (**E**), HBPI-IHC in PanINs and benign ducts (**F**), and HBPI-IHC in PDAC, benign ducts (inset, **G'**), islet cells (\*), and acinar units (\*\*; **G**) in a murine PDAC model. The arrowhead indicates an HBPI positive material in the lumens of glandular cancer groups (**G'**). Size bar is 100  $\mu$ m.

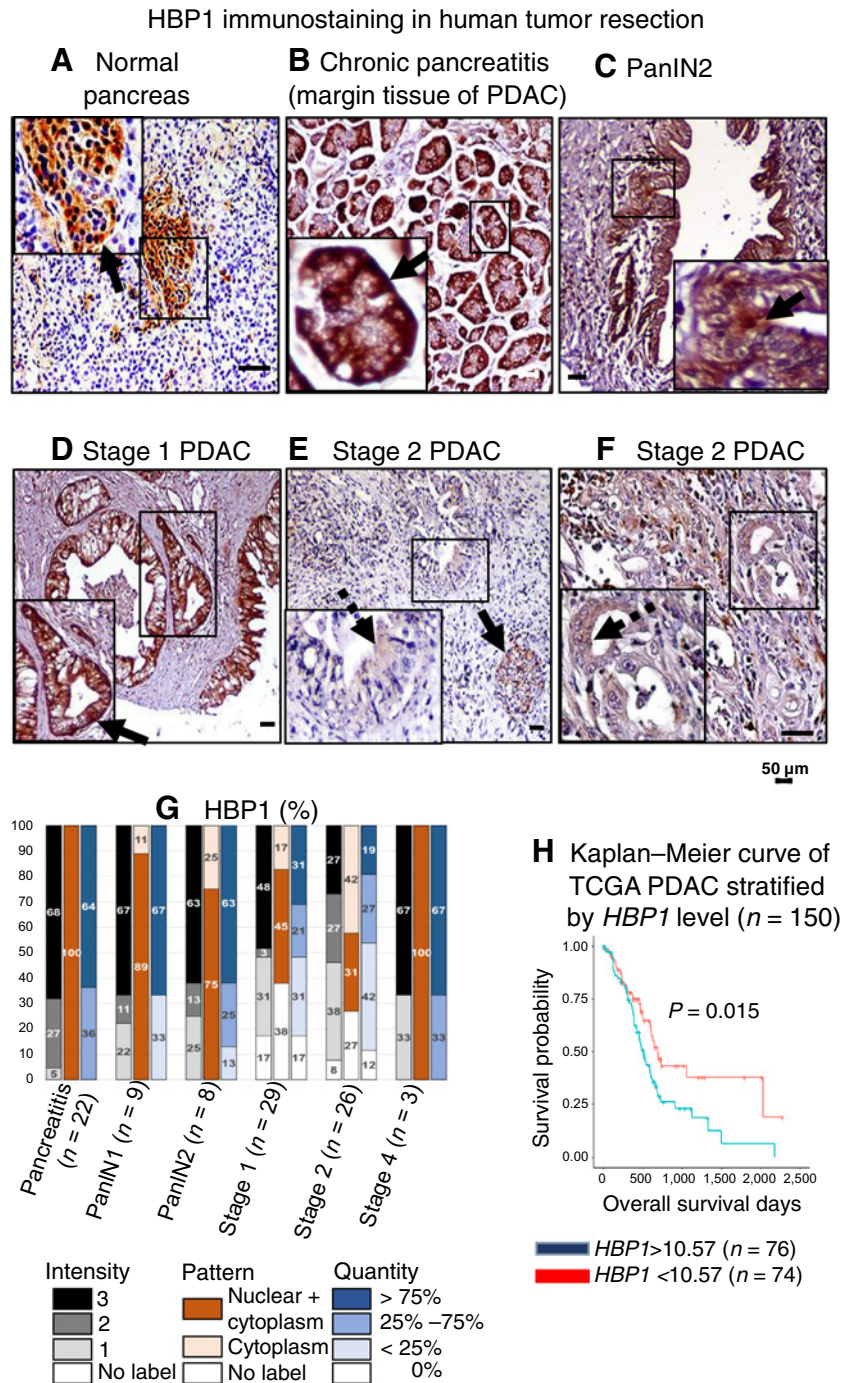
Supplementary Table S4). Apparent HBP1 targets included genes involved in cell migration, including neuron differentiation (Fig. 4C; FDR < 0.05). Indeed, HBP1 is known to regulate neuronal lineage differentiation (56). Consistently, cell migration-related pathways were ranked top among genes whose expression correlated with the HBP1 mRNA level in TCGA PDAC RNA-seq dataset (57) and cellular response to DNA damage as expected (Fig. 4D; FDR < 0.01; ref. 55).

Next, we examined the expression of HBP1 protein in the pancreata of mice (25) bearing PanINs and PDAC and in human pancreatic

cancer tissues (Supplementary Fig. S7A). HBP1 was barely detectable in the benign ductal epithelium (Fig. 4E and F), acinar cells (Fig. 4G, \*\*), and islet cells (Fig. 4G, \*). In contrast, HBP1 was strongly labeled in both nucleus and cytoplasm/membranes of PanINs (Fig. 4F) and slightly diffusely labeled in PDAC cells (Fig. 4G), except for budding cancers within the lumens of PDAC (Fig. 4G–G', arrowheads; n = 3). In humans, HBP1 protein was detected mainly in islet cells of the healthy pancreas (Fig. 5A, arrow) and the acinar compartments of chronic pancreatitis tissues adjacent to PDAC (n = 22/22; Fig. 5B, arrow). The HBP1 antibody labeled the ductal region of PanINs (n =

**Figure 5.**

HBP1 in human pancreata (see Supplementary Table S7B). HBP1-IHC in normal human pancreata (A), chronic pancreatitis at the margin of PDAC (B), PanIN2 (C), stage 1 PDAC (D), stage 2 PDAC (E), and another stage 2 PDAC (F). Boxes show a magnified view, arrows indicate positive staining, and dashed arrows indicate cytoplasmic diffused/weaker signal. Scale bars indicate 50 μm. G, Semi-quantification of HBP1-IHC in chronic pancreatitis (n = 22), PanIN1 (n = 9) and PanIN2 (n = 8), and various stages of PDAC (stage 1, n = 29; stage 2, n = 26; stage 4, n = 3). Left bars indicate % of samples with indicated staining intensity, 0: barely, 1: weakly, 2: moderately, and 3: intensely. Middle bars indicate % of samples with indicated staining patterns. Right bars indicate % of samples with indicated % area of investigation stained positively. H, Overall survival curve of TCGA PDAC patients (n = 150) stratified by the HBP1 mRNA level in their PDAC.



14/17; Fig. 5C) and a subset of PDAC with various degrees of intensity yet slightly diffused patterns (Fig. 5D–G). Notably, high *HBP1* mRNA levels in PDAC were correlated with poor patient prognosis ( $n = 150$ , TCGA PDAC; Fig. 5H). Altogether, we identified *HBP1* as a feature of the cell migration phenotype and transient neural gene expression pattern during PDAC progression and a potential biomarker for prognosis.

### HBP1 derepresses cell migratory genes and drives cell proliferation

To understand how elevated *HBP1* expression impacts pancreatic cell functions, we performed RNA-seq to define DE genes in a normal pancreatic epithelial cell line (H6C7) before (parental) and after overexpressing *HBP1* (*HBP1*-OE) or with the backbone control vector (CV; Supplementary Fig. S7B). Consistent with prior studies (55), mRNAs for cell-cycle regulators were significantly increased in *HBP1*-OE compared with controls (Fig. 6A and B, yellow cluster). Genes encoding growth factors, including receptor tyrosine kinases (RTK), were also upregulated in *HBP1*-OE, suggesting that aberrant *HBP1* can trigger cell proliferation (Fig. 6A and B, blue cluster).

In support of results obtained from 10-22 cells, a group of genes enriched in ECM disassembly and axon guidance was significantly upregulated in *HBP1*-OE (Fig. 6A and B, blue cluster). In contrast, genes enriched in type I IFN pathways or ncRNA processing were significantly downregulated in *HBP1*-OE (Supplementary Fig. S6A, purple and red clusters). Altogether, the aberrant expression of *HBP1* can induce cell migratory and proliferation pathways in normal pancreas cells.

Among human PDAC cell lines examined, the AsPC1 line expresses a high level of *HBP1* mRNA (Fig. 6C). Thus, AsPC-1 cells were introduced with two CRISPR-Cas9 gRNAs to disrupt *HBP1* or with CRISPR-Cas9 control vectors. As *HBP1* requires RB binding for its function (58), we designed two gRNAs targeting its domain that binds to RB1 (Fig. 6D; ref. 55). gRNA#1 almost completely disrupted RB1-binding sites, but gRNA#2 did not (Fig. 6D). We then determined the proliferation rate of AsPC-1 cells with the ATP levels that are proportional to the number of cells and the invasion rate with the number of cells migrated through matrigel. *HBP1* knockout cells (gRNA#1) had significantly reduced proliferation by 30% and invasiveness by 50%, compared with control AsPC-1 cells (Cas9; Fig. 6E and F). As expected, AsPC-1 gRNA#2 cells had lesser reduced proliferation and invasiveness (Fig. 6E and F). Conversely, ectopic expression of *HBP1* (OE) in Miapaca2 cells, which express a low level of the endogenous *HBP1*, slightly increased invasion (Fig. 6G and H) and moderately increased proliferation ( $P < 0.05$ ; Fig. 6I) compared with control cells with the backbone vector (CV). Altogether, these results suggest that aberrant expression of *HBP1* increases cell proliferation and migration by upregulating the RTK pathway, axon guidance, and ECM remodeling genes during PDAC progression.

### BACH1 and RUNX3 associate with PDAC progression features

*BACH1*/*MAFK* and *RUNX* motifs were the highest-ranked at promoters of group 5 genes (Fig. 7A and B; Supplementary Table S4). *BACH1* forms a heterodimer with small MAF proteins such as *MAFK* to repress transcription (59). While *MAFK* was constitutively expressed across timepoints after differentiation (Supplementary Fig. S7C), the expression of *BACH1* was variable throughout the time course and increased at the 9 months stage (Fig. 7C). Genes with a *BACH1* binding motif were involved in degranulation/intracellular vesicle tracking (Fig. 7E). Proteins encoded by one-third of *BACH1* target genes were identified in urine

exosomes (FDR  $< 0.05$ ; ref. 60). Patients with a high level of *BACH1* mRNA in PDAC also had a worse prognosis in TCGA dataset (Fig. 7F), indicating that *BACH1* may impact PDAC prognosis. The *BACH1* protein was expressed mainly in islet cells of the normal human pancreas (Fig. 7G, arrows) and in acinar and ductal cells in chronic pancreatitis ( $n = 14/21$  in the cytoplasm; Fig. 7H), but not in stromal cells in either. *BACH1* was detected in both ductal and stromal cells in PanINs ( $n = 17$ ) and PDAC of all stages ( $n = 8$ ; Fig. 7I–M).

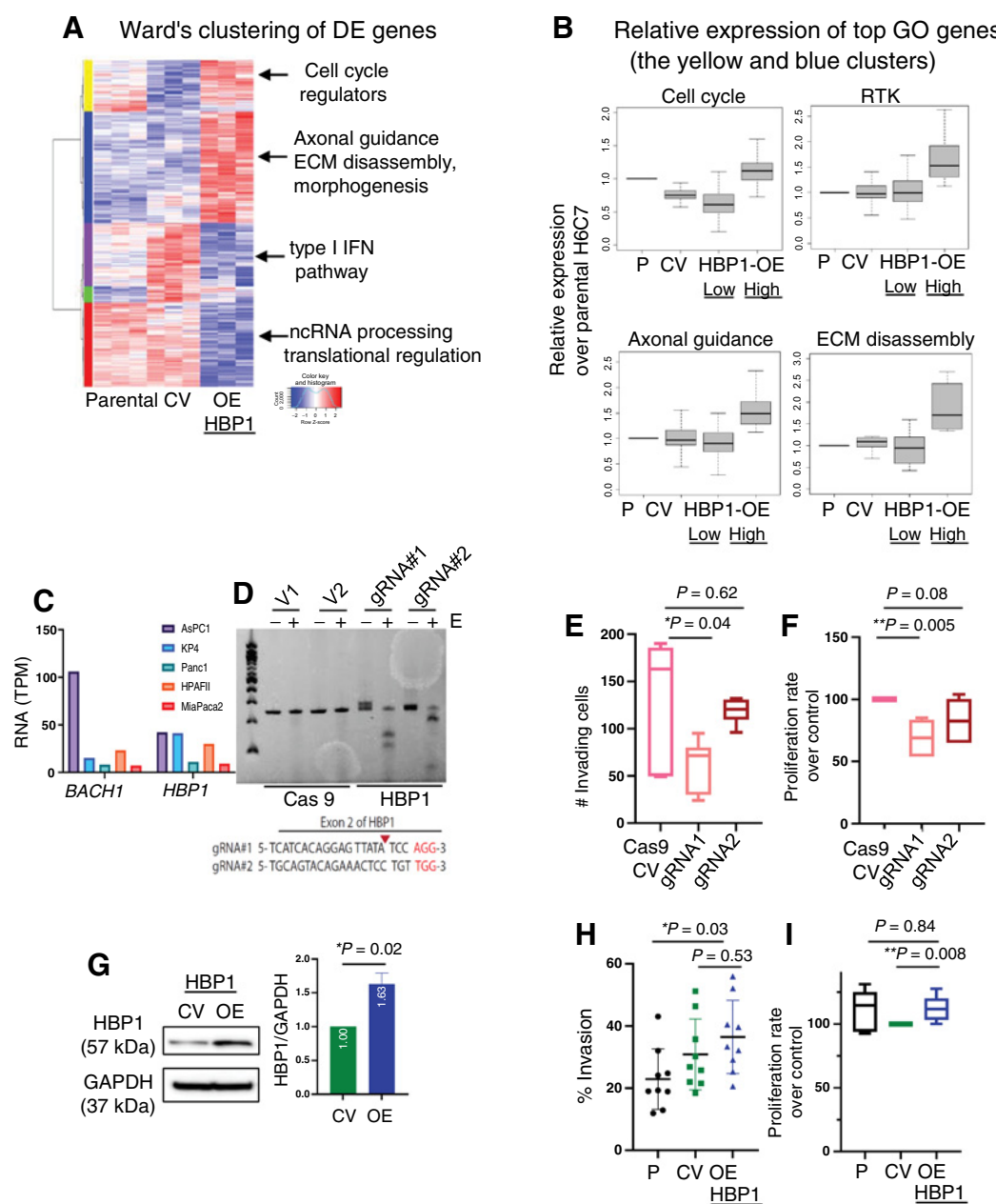
Among proteins that bind to the *RUNX* motif, *RUNX1* and *RUNX3* were expressed late in PDAC progression (Supplementary Fig. S7C) and the expression of *RUNX3*, a transcriptional repressor (61), was inversely associated with the expression of group 5 genes (Fig. 7D). Most promoters harboring the *RUNX* motif were of genes involved in vesicle transport ( $q < 0.01$ ) and encoding proteins found in cancer-specific exosomes ( $n = 7/9$ , asterisks; Fig. 7N; ref. 62). Indeed, genes whose expression negatively correlate with the *RUNX3* mRNA level in the PDAC TCGA (Pearson Correlation  $> 0.2$ ) were most enriched in the endosome transport with multivesicular body assembly and Endosomal Sorting Complex Required for Transport (ESCRT; ref. 63; FDR  $< 0.05$ ; Supplementary Table S3H).

## Discussion

Herein, we use the 10-22 cell model to provide the first transcriptional characterization of an isogenic trajectory of ductal cells in human PDAC development. We showed that 10-22 cells exhibit ESC gene signatures while retaining signatures of the polarized epithelial lineage from which they were derived under pluripotency culture conditions, explaining their preference to undergo PDAC development upon differentiation in mice. Reflecting their endogenous genetic alterations in *KRAS*, *TP53*, and *CDKN2A*, 10-22 cells exhibit basal subtype gene signatures soon after being released from pluripotency, yet classical ductal gene programs eventually take over.

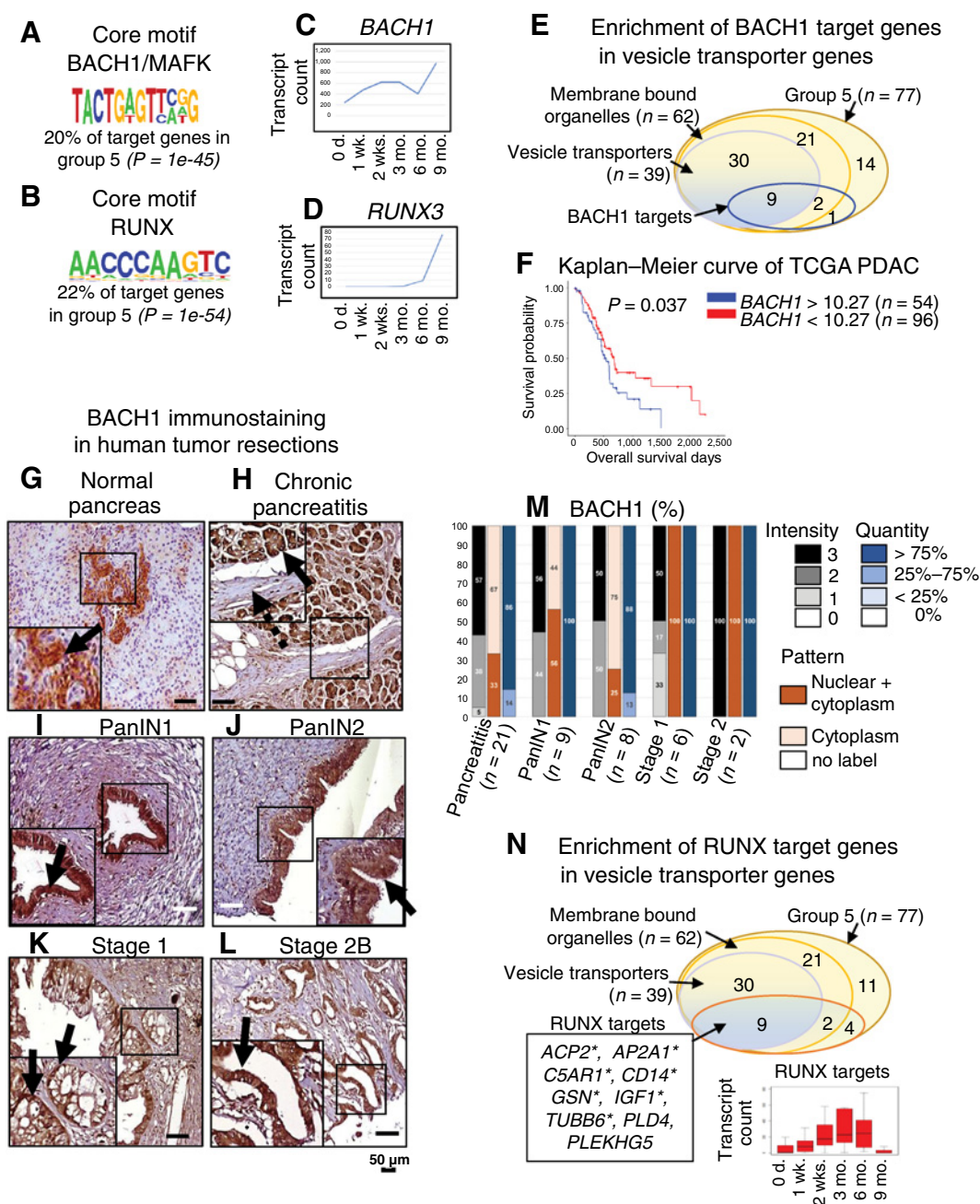
Neuronal differentiation and neural stem cell proliferation genes were upregulated during early PDAC progression, implying that a neuronal differentiation program may trigger cell migration early during PDAC progression. Indeed, genetic alterations in axon guidance are observed in human PDAC (64). Perineural invasion, an unfavorable prognostic marker, is common in patients (65, 66). Perineural invasions did not correlate with tumor size and 75% of stage I PDAC cases were accompanied by neural invasion (65). These clinical observations support our finding that perineural invasion may contribute to early invasion or dissemination.

Extracellular vesicles function as mediators in cellular contact (67), and PDAC-derived exosomes induce a pre-metastatic niche formation in naïve mice (68). We found that the gene signature for extracellular vesicles was transiently upregulated in PanIN and early PDAC and significant enrichment of Notch and Hedgehog pathways, which are implicated in exosome formation (63), in early PDAC progression of the 10-22 model (Supplementary Table S5). However, genes encoding extracellular vesicles are downregulated with the concomitant increase of the repressor *RUNX3* (69). Indeed, most genes harboring a *RUNX* motif relate to cancer-specific exosomes (Fig. 7N; ref. 62). *RUNX3* expression is negatively correlated with endosome transport genes via ESCRT, which is required to form a subset of exosomes (Supplementary Table S3H; ref. 63). Thus, our longitudinal transcriptome analysis uncovered transient gene signatures that could be masked at later stages by a regulator needed for PDAC. In contrast, *BACH1* is a negative regulator of oxidative stress-induced response (59). The *BACH1* level correlates with PDAC stages and



**Figure 6.**

HBP1 increases cell migration and proliferation. **A**, Ward clustering of DE genes across parental, control GFP vector (CV), and HBP1-overexpressing H6C7 cells (OE;  $FDR < 0.05$  by LRT). The heatmap indicates Z-score gene expression. Representative top GO in each cluster is described. **B**, Relative expression of top GO genes of the yellow and blue clusters, which are upregulated DE genes in HBP1-overexpressing H6C7 cells. Cell-cycle regulator genes ( $n = 107$ ) are enriched in the yellow cluster, and RTK ( $n = 85$ ), axonal guidance ( $n = 117$ ), and ECM disassembly ( $n = 10$ ) genes are enriched in the blue cluster. **C**, *HBP1* and *BACH1* mRNA levels in human PDAC cell lines shown as Transcripts Per Million (TPM) obtained from Expression Atlas. **D**, Validation of indel mutations in *HBP1* exon 2 in AsPC-1 cells targeted with CRISPR-Cas9 with two guide RNA (gRNA)s or CRISPR-Cas9 controls ("V1" and "V2") by T7 Endonuclease I treatment. Sequences of guide RNA #1 and #2, cutting the neighboring sequences to the RB-binding domain of HBP1 exon 2. **E**, Invasion assay at 36 hours post-plating AsPC-1 cells targeted with CRISPR-Cas9 control (Cas9 CV) or the indicated *HBP1* gRNAs. Y-axis indicates the number of invading cells (technical replicates  $n = 6$ ; \*,  $P = 0.04$ ). **F**, Proliferation assay at 48 hours post-plating AsPC-1 cells targeted with CRISPR-Cas 9 controls or the indicated *HBP1* gRNAs. Data are shown as a box-and-whisker plot with a median from six independent technical replicates. Y-axis shows the proliferation rate of gRNAs cells over the control cells. \*\*,  $P < 0.005$ . **G**, Western blot image of HBP1 expression in MiaPaca2 cell expressing HBP1 (OE) and control vector (CV). Bar graph shows normalized HBP1 levels over GAPDH ( $P = 0.0226$ ,  $n = 3$  paired  $t$  test). Invasion assay (**H**, one-way ANOVA with multiple comparisons,  $n = 9$ ; \*,  $P = 0.0384$ ) and proliferation assay (**I**, unpaired  $t$  test with Welch correction,  $n = 8$ ; \*\*,  $P = 0.0081$ ) of parental (P) and MiaPaca2 cells transduced with lentiviruses expressing control GFP vector (CV) or HBP1 vectors ("OE").

**Figure 7.**

BACH1 and RUNX3 as upstream regulators of genes associated with the early lesions to invasive stages. BACH1/MAFK (**A**) and RUNX (**B**) motifs. *BACH1* (**C**) and *RUNX3* (**D**) expressions during PDAC progression of 10–22 KiR-EG cells. **E**, Venn diagram of group 5 genes with BACH1 target genes. **F**, Kaplan–Meier survival curve of TCGA PDAC patients stratified by *BACH1* mRNA level ( $n = 150$ ). BACH1-IHC in normal human pancreata (**G**), chronic pancreatitis at the margin of PDAC (**H**), ductal compartment in PanIN1 (**I**) and PanIN2 (**J**), and stage 1 (**K**) and stage 2B (**L**) PDAC. Boxes show a magnified view, arrows indicate positive staining, and dashed arrows indicate cytoplasmic diffused/weaker signal. Scale bars indicate 50  $\mu\text{m}$ . **M**, Semi-quantification of BACH1-IHC in chronic pancreatitis ( $n = 21$ ), PanIN1 ( $n = 9$ ) and PanIN2 ( $n = 8$ ), and PDAC ( $n = 6$  in stage 1,  $n = 2$  in stage 2). Left bars indicate % of samples with indicated staining intensity, 0: barely, 1: weakly, 2: moderately, and 3: intensely. Middle bars indicate % of samples with indicated staining patterns. Right bars indicate % of samples with indicated % area of investigation stained positively (see Supplementary Table S7C for IHC quantification). **N**, Venn diagram of vesicle transporter genes and RUNX target genes. Asterisks denote RUNX target genes identified in cancer-specific exosomes.

high *BACH1* mRNA levels associate with human PDAC patients' poor prognosis. Ectopic *BACH1* expression in Miapaca 2 cells showed increased invasiveness and decreased proliferation (Supplementary Fig. S7D–S7G). A polymorphism in the *BACH1* locus has been

associated with increased pancreatic cancer risk (70), and a chimeric *BACH1* transcript has been identified in a patient's PDAC (16). *BACH1* was reported to promote epithelial-to-mesenchymal transition and metastasis of PDAC (71), implying PDAC promoting roles.

Intriguingly, HBP1 is transiently expressed in early PDAC in both the 10-22 model and human clinical samples (Figs. 4B, 5A–G). Survival analyses (Fig. 5H) and our functional tests (Fig. 6) indicate a negative role of HBP1 in patients' prognosis. Further studies are needed to unveil how HBP1 regulates pancreatic cell migration and confers neuronal migratory phenotypes and how these signaling influence PDAC progression. On the other hand, ectopic expression of HBP1 delays cells entering S-phases by prolonging the G<sub>1</sub>-phase, where cells respond to extracellular growth pathways. Indeed, we found that various RTK genes were simultaneously upregulated with cell-cycle regulators in the HBP1-overexpressing H6C7 cells (Fig. 6B). However, the effect of HBP1 on cell proliferation appears to depend on cell types (72–74). Deleterious mutations in *HBPI* are observed frequently in breast cancers (72) but rarely in PDAC. Instead, focal *HBPI* amplification is observed in 2.7% TCGA PDAC (57), implying a tumor-promoting role for HBP1 in PDAC.

In summary, our longitudinal transcriptome study using the 10-22 cell model shows that HBP1, RUNX3, and BACH1 may regulate distinct pathophysiologic features during PDAC progression. Further investigation is required to dissect whether they can serve as potential therapeutic targets during PDAC progression.

### Authors' Disclosures

J. Kim reports grants from Medical Research Foundation New Investigator Grant and CRUK-OHSU Project Award during the conduct of the study. No disclosures were reported by the other authors.

### References

1. Hezel AF, Kimmelman AC, Stanger BZ, Bardeesy N, Depinho RA. Genetics and biology of pancreatic ductal adenocarcinoma. *Genes Dev* 2006;20:1218–49.
2. Basturk O, Hong SM, Wood LD, Adsay NV, Albores-Saavedra J, Biankin AV, et al. A revised classification system and recommendations of the baltimore consensus meeting for neoplastic precursor lesions in the pancreas. *Am J Surg Pathol* 2015;39:1730–41.
3. Kanda M, Matthaei H, Wu J, Hong SM, Yu J, Borges M, et al. Presence of somatic mutations in most early-stage pancreatic intraepithelial neoplasia. *Gastroenterology* 2012;142:730–3.
4. Murphy SJ, Hart SN, Lima JF, Kipp BR, Klebig M, Winters JL, et al. Genetic alterations associated with progression from pancreatic intraepithelial neoplasia to invasive pancreatic tumor. *Gastroenterology* 2013;145:1098–109.
5. Makohon-Moore AP, Matsukuma K, Zhang M, Reiter JG, Gerold JM, Jiao Y, et al. Precancerous neoplastic cells can move through the pancreatic ductal system. *Nature* 2018;561:201–5.
6. Hosoda W, Chianchiano P, Griffin JF, Pittman ME, Brosens LA, Noe M, et al. Genetic analyses of isolated high-grade pancreatic intraepithelial neoplasia (HG-PanIN) reveal paucity of alterations in TP53 and SMAD4. *J Pathol* 2017;242:16–23.
7. Buchholz M, Braun M, Heidenblut A, Kestler HA, Kloppel G, Schmiegel W, et al. Transcriptome analysis of microdissected pancreatic intraepithelial neoplastic lesions. *Oncogene* 2005;24:6626–36.
8. Crnogorac-Jurcevic T, Chelala C, Barry S, Harada T, Bhakta V, Lattimore S, et al. Molecular analysis of precursor lesions in familial pancreatic cancer. *PLoS One* 2013;8:e54830.
9. Prasad NB, Biankin AV, Fukushima N, Maitra A, Dhara S, Elkahlon AG, et al. Gene expression profiles in pancreatic intraepithelial neoplasia reflect the effects of Hedgehog signaling on pancreatic ductal epithelial cells. *Cancer Res* 2005;65:1619–26.
10. Badea L, Herlea V, Dima SO, Dumitrascu T, Popescu I. Combined gene expression analysis of whole-tissue and microdissected pancreatic ductal adenocarcinoma identifies genes specifically overexpressed in tumor epithelia. *Hepatology* 2008;55:2016–27.
11. Grutzmann R, Pilarsky C, Ammerpohl O, Luttges J, Bohme A, Sipos B, et al. Gene expression profiling of microdissected pancreatic ductal carcinomas using high-density DNA microarrays. *Neoplasia* 2004;6:611–22.

### Authors' Contributions

**J. Kim:** Conceptualization, data curation, formal analysis, supervision, funding acquisition, validation, investigation, visualization, methodology, writing—original draft, project administration, writing—review and editing. **T. Ekstrom:** Formal analysis, validation, investigation, methodology, writing—review and editing. **W. Yang:** Validation, investigation, methodology. **G. Donahue:** Data curation, software, formal analysis. **D. Grygoryev:** Data curation, formal analysis, methodology. **T.T.M. Ngo:** Data curation, software. **J.L. Muschler:** Resources. **T. Morgan:** Formal analysis, visualization. **K.S. Zaret:** Conceptualization, supervision, funding acquisition, investigation, project administration, writing—review and editing.

### Acknowledgments

The work was supported by grants from the Institute for Regenerative Medicine (IRM) at the University of Pennsylvania (UPenn), the Translational Center of Excellence from the Abramson Cancer Center (UPenn), Medical Research Foundation New Investigator Grant (GCNCR1042A, to J. Kim), and CRUK-OHSU Project Award (2018-CRUK-OHSU-001, to J. Kim). We thank the IRM's ES cell core facility, the UPenn Stem Cell & Xenograft Core, the UPenn Small Animal Imaging Facility, and the MPI Core of the Center for Molecular Studies in Digestive and Liver Diseases (NIH/NIDDK P30-DK050306). This article was edited at Life Science Editors.

The costs of publication of this article were defrayed in part by the payment of page charges. This article must therefore be hereby marked *advertisement* in accordance with 18 U.S.C. Section 1734 solely to indicate this fact.

Received June 22, 2021; revised July 17, 2021; accepted July 26, 2021; published first July 30, 2021.

12. Collisson EA, Sadanandam A, Olson P, Gibb WJ, Truitt M, Gu S, et al. Subtypes of pancreatic ductal adenocarcinoma and their differing responses to therapy. *Nat Med* 2011;17:500–3.
13. Moffitt RA, Marayati R, Flate EL, Volmar KE, Loeza SG, Hoadley KA, et al. Virtual microdissection identifies distinct tumor- and stroma-specific subtypes of pancreatic ductal adenocarcinoma. *Nat Genet* 2015;47:1168–78.
14. Bailey P, Chang DK, Nones K, Johns AL, Patch AM, Gingras MC, et al. Genomic analyses identify molecular subtypes of pancreatic cancer. *Nature* 2016;531:47–52.
15. Chan-Seng-Yue M, Kim JC, Wilson GW, Ng K, Figueroa EF, O'Kane GM, et al. Transcription phenotypes of pancreatic cancer are driven by genomic events during tumor evolution. *Nat Genet* 2020;52:231–40.
16. Liang WS, Craig DW, Carpten J, Borad MJ, Demeure MJ, Weiss GJ, et al. Genome-wide characterization of pancreatic adenocarcinoma patients using next generation sequencing. *PLoS One* 2012;7:e43192.
17. Argani P, Rosty C, Reiter RE, Wilentz RE, Murugesan SR, Leach SD, et al. Discovery of new markers of cancer through serial analysis of gene expression: prostate stem cell antigen is overexpressed in pancreatic adenocarcinoma. *Cancer Res* 2001;61:4320–4.
18. Iacobuzio-Donahue CA, Maitra A, Shen-Ong GL, van Heek T, Ashfaq R, Meyer R, et al. Discovery of novel tumor markers of pancreatic cancer using global gene expression technology. *Am J Pathol* 2002;160:1239–49.
19. Notta F, Chan-Seng-Yue M, Lemire M, Li Y, Wilson GW, Connor AA, et al. A renewed model of pancreatic cancer evolution based on genomic rearrangement patterns. *Nature* 2016;538:378–82.
20. Ouyang Y, Pan J, Tai Q, Ju J, Wang H. Transcriptomic changes associated with DKK4 overexpression in pancreatic cancer cells detected by RNA-Seq. *Tumour Biol* 2016;37:10827–38.
21. Miyabayashi K, Baker LA, Deschenes A, Traub B, Caligiuri G, Plenker D, et al. Intraductal transplantation models of human pancreatic ductal adenocarcinoma reveal progressive transition of molecular subtypes. *Cancer Discov* 2020;10:1566–89.
22. Yachida S, Jones S, Bozic I, Antal T, Leary R, Fu B, et al. Distant metastasis occurs late during the genetic evolution of pancreatic cancer. *Nature* 2010;467:1114–7.
23. Campbell PJ, Yachida S, Mudie LJ, Stephens PJ, Pleasance ED, Stebbings LA, et al. The patterns and dynamics of genomic instability in metastatic pancreatic cancer. *Nature* 2010;467:1109–13.

24. Trapnell C, Cacchiarelli D, Grimsby J, Pokharel P, Li S, Morse M, et al. The dynamics and regulators of cell fate decisions are revealed by pseudotemporal ordering of single cells. *Nat Biotechnol* 2014;32:381–6.
25. Hingorani SR, Petricoin EF, Maitra A, Rajapakse V, King C, Jacobetz MA, et al. Preinvasive and invasive ductal pancreatic cancer and its early detection in the mouse. *Cancer Cell* 2003;4:437–50.
26. Aiello NM, Maddipati R, Norgard RJ, Balli D, Li J, Yuan S, et al. EMT subtype influences epithelial plasticity and mode of cell migration. *Dev Cell* 2018;45:681–95 e4.
27. Krahn NM, De La OJ, Swift GH, Hoang CQ, Willet SG, Pan FC, et al. The acinar differentiation determinant PTF1A inhibits initiation of pancreatic ductal adenocarcinoma. *Elife* 2015;4:e07125.
28. Roy N, Takeuchi KK, Ruggeri JM, Bailey P, Chang D, Li J, et al. PDX1 dynamically regulates pancreatic ductal adenocarcinoma initiation and maintenance. *Genes Dev* 2016;30:2669–83.
29. Schlesinger Y, Yosefov-Levi O, Kolodkin-Gal D, Granit RZ, Peters L, Kalifa R, et al. Single-cell transcriptomes of pancreatic preinvasive lesions and cancer reveal acinar metaplastic cells' heterogeneity. *Nat Commun* 2020;11:4516.
30. Kim J, Hoffman JP, Alpaugh RK, Rhim AD, Reichert M, Stanger BZ, et al. An iPSC line from human pancreatic ductal adenocarcinoma undergoes early to invasive stages of pancreatic cancer progression. *Cell Rep* 2013;3:2088–99.
31. Kim J, Bamlet WR, Oberg AL, Chaffee KG, Donahue G, Cao XJ, et al. Detection of early pancreatic ductal adenocarcinoma with thrombospondin-2 and CA19–9 blood markers. *Sci Transl Med* 2017;9:eaah5583.
32. Filonov GS, Piatkevich KD, Ting LM, Zhang J, Kim K, Verkhusha VV. Bright and stable near-infrared fluorescent protein for in vivo imaging. *Nat Biotechnol* 2011;29:757–61.
33. Brembeck FH, Rustgi AK. The tissue-dependent keratin 19 gene transcription is regulated by KGLF/KLF4 and Sp1. *J Biol Chem* 2000;275:28230–9.
34. Dobin A, Davis CA, Schlesinger F, Drenkow J, Zaleski C, Jha S, et al. STAR: ultrafast universal RNA-seq aligner. *Bioinformatics* 2013;29:15–21.
35. Love MI, Huber W, Anders S. Moderated estimation of fold change and dispersion for RNA-seq data with DESeq2. *Genome Biol* 2014;15:550.
36. Heinz S, Benner C, Spann N, Bertolino E, Lin YC, Laslo P, et al. Simple combinations of lineage-determining transcription factors prime cis-regulatory elements required for macrophage and B cell identities. *Mol Cell* 2010;38:576–89.
37. Cancer Genome Atlas Research Network. Integrated genomic characterization of pancreatic ductal adenocarcinoma. *Cancer Cell* 2017;32:185–203.
38. Goldman MJ, Craft B, Hastie M, Repecka K, McDade F, Kamath A, et al. Visualizing and interpreting cancer genomics data via the Xena platform. *Nat Biotechnol* 2020;38:675–8.
39. Xie R, Everett LJ, Lim HW, Patel NA, Schug J, Kroon E, et al. Dynamic chromatin remodeling mediated by polycomb proteins orchestrates pancreatic differentiation of human embryonic stem cells. *Cell Stem Cell* 2013;12:224–37.
40. Boon K, Osorio EC, Greenhut SF, Schaefer CF, Shoemaker J, Polyak K, et al. An anatomy of normal and malignant gene expression. *Proc Natl Acad Sci U S A* 2002;99:11287–92.
41. Salomonis N, Dexheimer PJ, Omberg L, Schroll R, Bush S, Huo J, et al. Integrated genomic analysis of diverse induced pluripotent stem cells from the Progenitor Cell Biology Consortium. *Stem Cell Reports* 2016;7:110–25.
42. Hruban RH, Maitra A, Goggins M. Update on pancreatic intraepithelial neoplasia. *Int J Clin Exp Pathol* 2008;1:306–16.
43. Argani P, Iacobuzio-Donahue C, Ryu B, Rosty C, Goggins M, Wilentz RE, et al. Mesothelin is overexpressed in the vast majority of ductal adenocarcinomas of the pancreas: identification of a new pancreatic cancer marker by serial analysis of gene expression (SAGE). *Clin Cancer Res* 2001;7:3862–8.
44. Muller FJ, Laurent LC, Kostka D, Ulitsky I, Williams R, Lu C, et al. Regulatory networks define phenotypic classes of human stem cell lines. *Nature* 2008;455:401–5.
45. Li J, Byrne KT, Yan F, Yamazoe T, Chen Z, Baslan T, et al. Tumor cell-intrinsic factors underlie heterogeneity of immune cell infiltration and response to immunotherapy. *Immunity* 2018;49:178–93.
46. Pinerio J, Bravo A, Queralt-Rosinach N, Gutierrez-Sacristan A, Deu-Pons J, Centeno E, et al. DisGeNET: a comprehensive platform integrating information on human disease-associated genes and variants. *Nucleic Acids Res* 2017;45:D833–D9.
47. Murtagh F, Legendre P. Ward's hierarchical agglomerative clustering method: which algorithms implement ward's criterion? *J Classification* 2014;31:274–95.
48. Smith CL, Goldsmith CA, Eppig JT. The Mammalian Phenotype Ontology as a tool for annotating, analyzing and comparing phenotypic information. *Genome Biol* 2005;6:R7.
49. Commisso C, Davidson SM, Soydaner-Azeloglu RG, Parker SJ, Kamphorst JJ, Hackett S, et al. Macropinocytosis of protein is an amino acid supply route in Ras-transformed cells. *Nature* 2013;497:633–7.
50. Yang S, Wang X, Contino G, Liesa M, Sahin E, Ying H, et al. Pancreatic cancers require autophagy for tumor growth. *Genes Dev* 2011;25:717–29.
51. Perera RM, Stoykova S, Nicolay BN, Ross KN, Fitamant J, Boukhali M, et al. Transcriptional control of autophagy-lysosome function drives pancreatic cancer metabolism. *Nature* 2015;524:361–5.
52. Melo SA, Luecke LB, Kahlert C, Fernandez AF, Gammon ST, Kaye J, et al. Glypican-1 identifies cancer exosomes and detects early pancreatic cancer. *Nature* 2015;523:177–82.
53. Schioppa T, Uranchimeg B, Saccani A, Biswas SK, Doni A, Rapisarda A, et al. Regulation of the chemokine receptor CXCR4 by hypoxia. *J Exp Med* 2003;198:1391–402.
54. Marchesi F, Piemonti L, Fedele G, Destro A, Roncalli M, Albarello L, et al. The chemokine receptor CX3CR1 is involved in the neural tropism and malignant behavior of pancreatic ductal adenocarcinoma. *Cancer Res* 2008;68:9060–9.
55. Tevosian SG, Shih HH, Mendelson KG, Sheppard KA, Paulson KE, Yee AS. HBP1: a HMG box transcriptional repressor that is targeted by the retinoblastoma family. *Genes Dev* 1997;11:383–96.
56. Watanabe N, Kageyama R, Ohtsuka T. Hbp1 regulates the timing of neuronal differentiation during cortical development by controlling cell cycle progression. *Development* 2015;142:2278–90.
57. Hoadley KA, Yau C, Wolf DM, Cherniack AD, Tamborero D, Ng S, et al. Multiplatform analysis of 12 cancer types reveals molecular classification within and across tissues of origin. *Cell* 2014;158:929–44.
58. Shih HH, Tevosian SG, Yee AS. Regulation of differentiation by HBP1, a target of the retinoblastoma protein. *Mol Cell Biol* 1998;18:4732–43.
59. Sun J, Hoshino H, Takaku K, Nakajima O, Muto A, Suzuki H, et al. Hemoprotein Bach1 regulates enhancer availability of heme oxygenase-1 gene. *EMBO J* 2002;21:5216–24.
60. Gonzales PA, Pisitkun T, Hoffert JD, Tchapyjnikov D, Star RA, Kleta R, et al. Large-scale proteomics and phosphoproteomics of urinary exosomes. *J Am Soc Nephrol* 2009;20:363–79.
61. Inoue KI, Ito K, Osato M, Lee B, Bae SC, Ito Y. The Transcription factor Runx3 represses the neurotrophin receptor TrkB during lineage commitment of dorsal root ganglion neurons. *J Biol Chem* 2007;282:24175–84.
62. Mathivanan S, Simpson RJ. ExoCarta: a compendium of exosomal proteins and RNA. *Proteomics* 2009;9:4997–5000.
63. McGough IJ, Vincent JP. Exosomes in developmental signalling. *Development* 2016;143:2482–93.
64. Biankin AV, Waddell N, Kassahn KS, Gingras MC, Muthuswamy LB, Johns AL, et al. Pancreatic cancer genomes reveal aberrations in axon guidance pathway genes. *Nature* 2012;491:399–405.
65. Pour PM, Bell RH, Batra SK. Neural invasion in the staging of pancreatic cancer. *Pancreas* 2003;26:322–5.
66. Chatterjee D, Katz MH, Rashid A, Wang H, Iuga AC, Varadhachary GR, et al. Perineural and intraneural invasion in posttherapy pancreaticoduodenectomy specimens predicts poor prognosis in patients with pancreatic ductal adenocarcinoma. *Am J Surg Pathol* 2012;36:409–17.
67. Tkach M, Thery C. Communication by extracellular vesicles: where we are and where we need to go. *Cell* 2016;164:1226–32.
68. Costa-Silva B, Aiello NM, Ocean AJ, Singh S, Zhang H, Thakur BK, et al. Pancreatic cancer exosomes initiate pre-metastatic niche formation in the liver. *Nat Cell Biol* 2015;17:816–26.
69. Whittle MC, Izeradjene K, Rani PG, Feng L, Carlson MA, DelGiorno KE, et al. RUNX3 controls a metastatic switch in pancreatic ductal adenocarcinoma. *Cell* 2015;161:1345–60.
70. Wu C, Miao X, Huang L, Che X, Jiang G, Yu D, et al. Genome-wide association study identifies five loci associated with susceptibility to pancreatic cancer in Chinese populations. *Nat Genet* 2011;44:62–6.

71. Sato M, Matsumoto M, Saiki Y, Alam M, Nishizawa H, Rokugo M, et al. BACH1 promotes pancreatic cancer metastasis by repressing epithelial genes and enhancing epithelial-mesenchymal transition. *Cancer Res* 2020; 80:1279–92.
72. Paulson KE, Rieger-Christ K, McDevitt MA, Kuperwasser C, Kim J, Unanue VE, et al. Alterations of the HBP1 transcriptional repressor are associated with invasive breast cancer. *Cancer Res* 2007;67:6136–45.
73. Sanghvi VR, Mavrakis KJ, Van der Meulen J, Boice M, Wolfe AL, Carty M, et al. Characterization of a set of tumor suppressor microRNAs in T cell acute lymphoblastic leukemia. *Sci Signal* 2014;7:ra111.
74. He S, Yang S, Niu M, Zhong Y, Dan G, Zhang Y, et al. HMG-box transcription factor 1: a positive regulator of the G1/S transition through the Cyclin-CDK-CDKI molecular network in nasopharyngeal carcinoma. *Cell Death Dis* 2018;9:100.